CHINESE OPTICS LETTERS

Vol. 20, No. 3 | March 2022

High peak power femtosecond cylindrical vector beams generation in a chirped-pulse amplification laser system

Zexing Zhao (赵泽兴)[1], Hao Chen (陈 浩)[1], Ziming Zhang (张子鸣)[1], Jiatong Li (李佳桐)[1], Fangxiang Zhu (朱方祥)[1], Wei Wan (万 威)[2], Fei He (何 飞)[2], Huifeng Wei (韦会峰)[2], Kangkang Chen (陈抗抗)[2], and Peiguang Yan (闫培光)[1*]

[1] College of Physics and Optoelectronic Engineering, Shenzhen University, Shenzhen 518060, China

[2] Wuhan Yangtze Soton Laser Photonics Co., Ltd., Wuhan 430205, China

*Corresponding author: yanpg@szu.edu.cn

Received November 27, 2021 | Accepted December 13, 2021 | Posted Online January 4, 2022

Cylindrical vector beams (CVBs), with non-uniform state of polarizations, have become an indispensable tool in many areas of science and technology. However, little research has explored high power CVBs at the femtosecond regime. In this paper, we report on the generation of high quality CVBs with high peak power and femtosecond pulse duration in a fiber chirped-pulse amplification laser system. The radially (azimuthally) polarized vector beam has been obtained with a pulse duration of 440 fs (430 fs) and a maximum average output power of 20.36 W (20.12 W). The maximum output pulse energy is ~20 μJ at a repetition rate of 1 MHz, corresponding to a high peak power of ~46 MW. The comparison between simulated intensity profiles and measured experimental results suggests that the generated CVBs have a remarkable intensity distribution. The proposed configuration of our laser system provides a promising solution for high quality CVBs generation with the characteristics of high peak power, ultrashort pulse duration, and high mode purity.

Keywords: femtosecond laser; structural beams; pulse shaping; amplifier.

DOI: 10.3788/COL202220.031405

1. Introduction

Cylindrical vector beams (CVBs) have attracted enormous scientific attention due to their unique optical properties, such as axially symmetric field amplitude distributions and radial or azimuthal polarization states, which enable imaging resolution below the diffraction limit and interact without the undesirable anisotropy produced by a linearly-polarized light[1–5]. A variety of applications utilizing CVBs have been explored such as high resolution imaging, nanoparticle manipulation, terahertz technology, data storage, and optical communication[6–11]. Generally, several typical optical devices, such as astigmatic mode converters (AMCs), liquid-crystal spatial light modulators (SLMs), and forked gratings, have been used as mode converters to transfer spatially homogeneous polarizations (e.g., linear or circular polarization) into spatially inhomogeneous cylindrical vector polarizations[12–16]. Although the abovementioned devices possess the property of spatially variant polarization of incident beams, they are restricted by high cost and low damage threshold for the high power laser system, which limits their practical applications. Additionally, a metasurface with a two-dimensional electromagnetic nanostructure has been used as an effective converter to simultaneously control the intensity, polarization, and phase of incident light. However, it also suffers from the small interaction area between light and nanostructures, complex fabrication process, and low damage threshold[17,18]. Recently, the spiral waveplate (S-waveplate) has attracted much attention due to its remarkable properties. Since the S-waveplate is fabricated in bulk fused silica with birefringent nanogratings by a femtosecond laser imprinting process, it owns a very high damage threshold ($> 20\,\mathrm{J\cdot cm^{-2}}$), large number aperture, and nearly 100% efficiency in polarization conversion, which is very suitable for use in high power laser systems to generate high quality CVBs with excellent output laser performance[19]. A linearly polarized Gaussian beam could be transferred into a CVB via the continuously varying slow axis direction of the S-waveplate to rotate the linear polarization with a designed angle and thus to produce a radial (azimuthal) distribution of the electric field[20]. In order to enhance the practical application ability of CVBs, output laser performance such as ultrashort pulse width, large peak power, high mode purity, and low amplitude fluctuations is quite required in the fields such as probing surface second-harmonic generation and near field microscopic imaging, especially femtosecond near field nanomachining of metals. However, CVBs with high peak power in the femtosecond regime have been little explored[21].

In this work, we report on a fiber chirped-pulse amplification (CPA) system combined with an S-waveplate to generate high

power femtosecond CVBs. The S-waveplate [RPC-1030-08, LIDT ~63.4 J/cm^2 at 1064 nm (10 ns); WORKSHOP] is used as an efficient mode converter behind the output port of the CPA system to convert a linearly polarized Gaussian mode into a higher-order Laguerre Gaussian mode, directly. We simulate the formation of radial and azimuthal vector beams using linear superposition of orthogonally polarized Hermite–Gaussian (HG) modes and demonstrate that the measured experimental results have high quality intensity distributions. The conversion efficiency of the mode conversion module is measured to be 97.3% for radially polarized beams and 96.1% for azimuthally polarized beams. After optimizing the laser system, the radially (azimuthally) polarized CVBs could be obtained with a pulse duration of 440 fs (430 fs) and a maximum average output power of 20.36 W (20.12 W). The maximum output pulse energy reaches ~20 μJ at a repetition rate of 1 MHz, corresponding to a peak power of ~46 MW.

2. Experiments and Methods

The diagram of a typical fiber CPA system with a CVB mode conversion module is shown in Fig. 1. The laser cavity can be divided into six parts. A homemade 1030 nm seed laser source is used with ~1 mW average output power and ~200 fs pulse duration. As shown in part I, a chirped-fiber-Bragg-grating (CFBG) stretcher with second and third-order dispersion compensation is incorporated into the laser cavity via a circulator to stretch the pulse duration of the seed laser. Part II is the first level amplification system containing wavelength division multiplexing (WDM, 980/1030) to inject pump power into the cavity, a section of single-clad ytterbium-doped fiber (YDF) as a gain medium, and an isolator to ensure the unidirectional propagation and avoid parasitic back-reflections. The pump source has a maximum power of 300 mW at 975 nm wavelength. Part III uses a section of double clad YDF as a gain medium for more efficient amplification of the incident laser. An optical combiner is utilized to inject a 975 nm multi-mode pump into the system with maximum pump power of 10 W. An isolator is also employed to prevent the effect of reverse transmitted light. A fiber pigtailed acoustic-optic modulator (AOM) is utilized behind the part III amplifier to remove inter-pulse amplified spontaneous emission (ASE) resulting from the prior core-pumped pre-amplifiers and adjust the laser repetition rates to optimize the laser performance. Behind the AOM is the fourth amplification system that includes a combiner to inject another 975 nm multi-mode pump with 20 W maximum output power and a part of the double clad YDF as well as an isolator. Then, the output pulses are compressed by a Treacy-type compressor based on two reflection gratings. The separation of gratings is optimized to match the stretcher and compensate the anomalous dispersion. The final average output power of our CPA system is 21 W with a pulse width of 461 fs assuming a sech^2 pulse shape. The repetition rate is set to be 1 MHz by the AOM. The output laser is a high quality Gaussian-shaped beam with a propagation parameter M^2 factor of 1.3 along with a slope efficiency of ~69%. In order to avoid the potential decline of mode quality of output CVBs induced by the S-waveplate inserted into the CPA system, after optimizing the output laser performance, the mode conversion module is embedded behind the output port of the CPA system for larger efficiency conversion and higher mode quality of the CVBs.

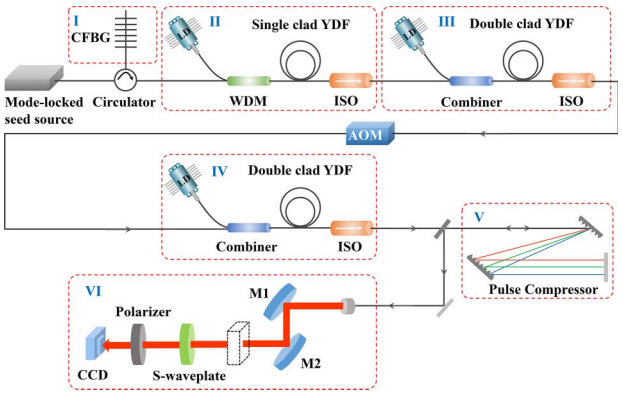

Fig. 1. Schematic of the generation of radially polarized and azimuthally polarized beams by a typical fiber CPA system. CFBG, chirped fiber Bragg grating; WDM, wavelength division multiplexer; ISO, isolator; AOM, acoustic-optical modulator; M1 and M2, reflective mirrors.

In theory, an incident Gaussian beam with an s-polarization state passing through a mode converter can be converted into a radial vector beam. In contrast, a p-polarized beam will be transferred into an azimuthal vector beam. In our experiment, the output Gaussian beam has an s-polarization state. The azimuthal vector beam could be obtained by inserting a half-wave plate shown in Part IV with a dashed box to convert an s-polarization into a p-polarization state. The relationship between the fast-axis orientation of the vector converter and azimuth angle is represented as $\theta = \alpha\varphi + \delta$, where δ is the fast-axis direction at $\varphi = 0$, and the value of m is set by $m = 2\alpha$. Therefore, the Jones matrix of converter can be described as follows[6]:

$$J(\varphi) = \begin{pmatrix} \cos(m\varphi) & \sin(m\varphi) \\ \sin(m\varphi) & -\cos(m\varphi) \end{pmatrix}. \quad (1)$$

The value of δ is zero, corresponding to the horizontal direction of the fast axis. As for $m = 1$, after multiplying a vector describing the s-polarized beam with the matrix of $\binom{1}{0}$, the final matrix for the radially polarized vector beam is depicted as $\begin{pmatrix} \cos(\varphi) \\ \sin(\varphi) \end{pmatrix}$. Similarly, the matrix for the p-polarized beam is $\binom{0}{1}$, corresponding to the matrix of the azimuthally polarized vector beam of $\begin{pmatrix} \sin(\varphi) \\ -\cos(\varphi) \end{pmatrix}$. Figure 2 is the simulated intensity profiles of orthogonally polarized modes and CVBs. In the theory, the linear superposition of the x-polarized HG_{01} mode and y-polarized HG_{01} mode can generate a radically polarized mode [Fig. 2(a)]. Similarly, a radially polarized mode can be formed by linear superposition of the x-polarized HG_{10} mode and y-polarized HG_{10} mode [Fig. 2(b)]. In order to examine

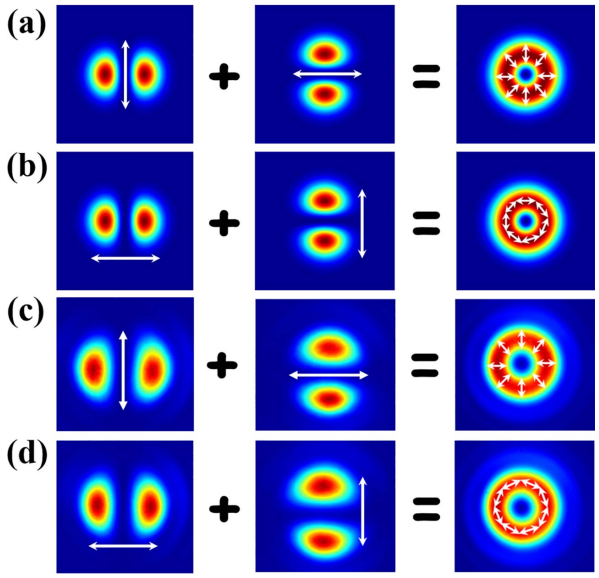

Fig. 2. (a) and (b) are the calculated intensity distribution for the formation of radial and azimuthal vector beams using linear superposition of orthogonally polarized HG modes. (c) and (d) are the measured intensity profiles by a CCD camera at maximum power.

the mode quality of CVBs generated in experiment, we record the intensity distribution of different modes by a CCD camera at maximum output power, as shown in Figs. 2(c) and 2(d). The results are in good agreement with the numerical simulations, which indicates high mode quality of our CVBs.

In our experiment, both the radial and azimuthal beams display a donut-shape beam with a typical intensity null at the beam center, which belongs to the first higher-order Laguerre Gaussian mode and is in good agreement with previous results[22]. Note that the slight intensity asymmetry of measured output vector beams is mainly caused by a wedge prism utilized in experiment to attenuate the incident energy on the detection area of the CCD camera. As for the radially polarized vector beam, it has high mode purity with a mode extinction ratio (MER) of ~20 dB by using the method proposed in Ref. [23].

3. Results

Figure 3(a) is the output optical spectra of the Gaussian beam and CVBs under the maximum output power measured by an optical spectrum analyzer (Yokogawa AQ6370C). The laser operates at a central wavelength of 1033.11 nm. The 3 dB bandwidths were measured as 4.69 nm, 4.74 nm, and 5.21 nm for the Gaussian beam and radial and azimuthal vector beams, respectively. According to the measured optical spectrum, there is no obvious ASE in the output optical spectra, which is effectively suppressed by an AOM employed in the CPA system. The result demonstrates that our CPA system has a great output laser performance. The final output beam has an optical signal-to-noise ratio (OSNR) of ~50.2 dB (radial vector beam) and ~48.1 dB (azimuthal vector beam). It should be noted that the final output

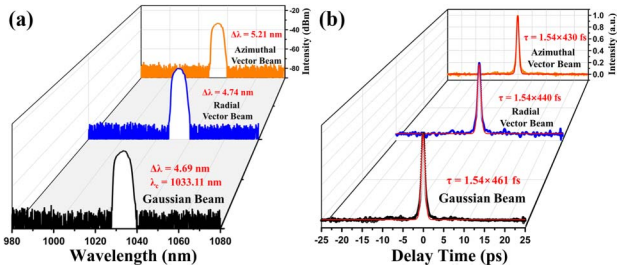

Fig. 3. Laser performance at maximum output power. (a) The optical spectra of the Gaussian beam and radial and azimuthal vector beams. (b) The autocorrelation trace with $sech^2$ fit.

spectrum is attenuated in order to measure the optical spectra at high power, which might introduce slight instabilities and further make an impact on 3 dB bandwidths. Figure 3(b) is the autocorrelation trace of pulse for the Gaussian beam, radial vector beam, and azimuthal vector beam under maximum output power by using a autocorrelator (APE Pulsecheck). The measured span is set to be 50 ps to further investigate the output pulse performance. The real pulse widths are calculated to be 461 fs, 430 fs, and 440 fs for the Gaussian beam, radial vector beam, and azimuthal vector beam after multiplying the de-correlation factor of 0.648 for the $sech^2$ pulse profile, respectively. Interestingly, as shown in Fig. 3(b), except for the fundamental frequency pulse signal, there are no multi-pulses state and significant pedestal observed in the whole trace, indicating that the laser operated at a single-pulse state with a high stability. Compared with the pulse width of the Gaussian beam, both the radical vector beam and azimuthal vector beam have slightly narrow pulse widths, which result from the negative dispersion introduced by the S-waveplate and optical elements in the mode conversion system.

As shown in Fig. 4, the intensity profiles of the vector beam passing through a rotated linear polarizer are recorded by a CCD

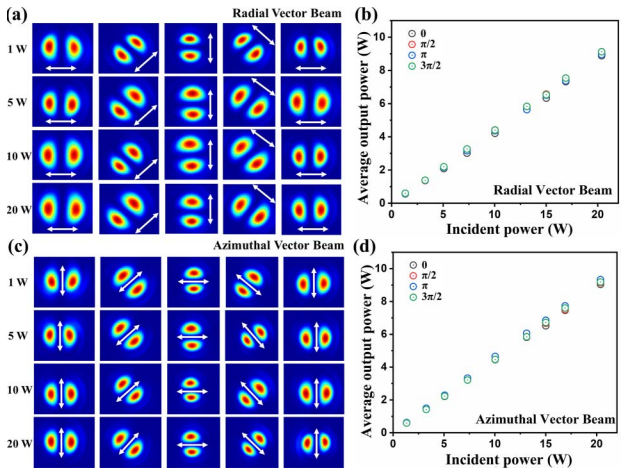

Fig. 4. Measured intensity profiles of the output vector beams after passing through a rotated linear polarizer at different output powers. (a) The radially polarized vector beam, with (b) the average output power. (c) The azimuthally polarized vector beam, with (d) the average output power. The white arrows exhibit the transmission axis of the polarizer.

camera. Figure 4(a) is the radially polarized vector beam and related intensity distribution with different angles of the transmission axis of the polarizer, while Fig. 4(c) corresponds to the azimuthally polarized vector beam and its intensity profiles under various angles with an average output power from 1 W to 20 W. The two-lobed intensity distribution under different angles of the linear polarizer has a good symmetrical distribution, which indicates that our radial and azimuthal vector beams own uniform intensity profiles. Different from the low damage threshold of other types of mode converters such as AMC, liquid-crystal SLM, and metasurface, all of them need to be embedded before the final amplifier of the CPA system to protect against destruction at high incident power. The shortage of the above approaches is easily causing the output beam to own an elliptical intensity profile, which results from the difficulty of aligning the vector beam with the optic axis of the slightly curved angle cleaved fiber end facet.

In order to further investigate the characteristics of CVBs, the average output power of the radial vector beam and azimuthal vector beam is measured at various incident powers of the Gaussian beam[24]. Both of them own a nearly linear relationship between incident power and output vector beam power, which demonstrates that our vector beams have a high stability. When the power of the incident Gaussian beam is increased to 21 W, corresponding to the maximum power in experiment, the output power of radial and azimuthal vector beams is measured to be 20.36 W and 20.12 W, respectively. Since the repetition rate of pulse trains is 1 MHz, the maximum pulse energy is calculated to be 20.36 μJ and 20.12 μJ. In addition, the maximum peak power is calculated to be 46.3 MW (radial vector beam) and 46.8 MW (azimuthal vector beam), which are two orders of magnitude higher than in previously reported research[11]. As shown in Fig. 5, the conversion efficiency of the mode converter is calculated to be 97.3% for the radially polarized beam and 96.1% for the azimuthally polarized beam. The very high conversion efficiency is mainly benefited from the near 100% polarization conversion and high transmission of the S-waveplate. In addition, the S-waveplate is placed behind the output port of the CPA system, ensuring high mode purity and symmetric intensity profiles of generated vector beams. Note that the conversion efficiency of the radial vector beam is a bit lower than that of the azimuthal vector beam. It is mainly caused by the insertion loss induced by a half-wave plate behind the output port of the CPA system to convert the Gaussian beam from the s-polarized state into the p-polarized state. Additionally, in Ref. [25], we found that the pulse duration of most CVBs stays on the order of picoseconds or even nanoseconds. Such femtoseconds laser uses a fused few-mode coupler[26,27] or two-mode fiber[28]. Compared with these works, our device generates ultrahigh peak power CVB femtosecond pulse laser more efficiently through the S-waveplate.

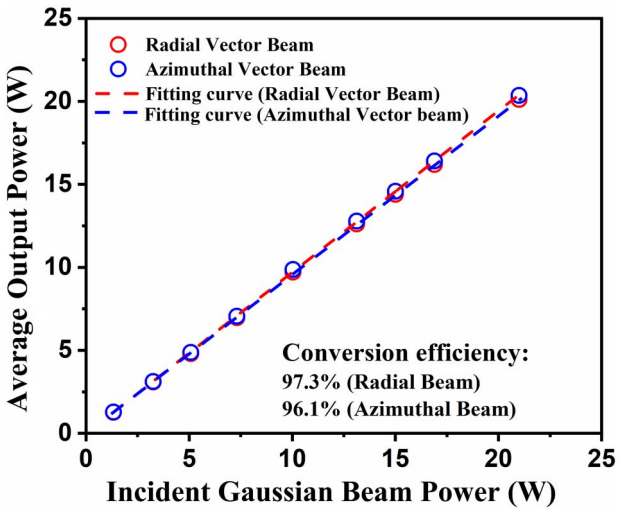

Fig. 5. Relationship between incident Gaussian beam power and vector beam power. The dot lines are the linear fitting curves. The insert picture is the intensity profiles of Gaussian beams captured by a CCD camera at maximum output power.

4. Conclusion

In summary, we report on the generation of radial and azimuthal vector beams in a fiber CPA laser system at the femtosecond regime with ~46 MW peak power and maximum pulse energy of ~20 μJ. The mode converter used in our experiment has a very high damage threshold that allows it to be placed directly on the output port of the CPA laser system without any other heat dissipation process, which is beneficial for high mode quality CVBs generation. In our experiment, the radially (azimuthally) polarized vector beam has a pulse duration of 440 fs (430 fs) and a maximum average output power of 20.36 W (20.12 W). Our proposed laser system configuration provides a promising solution for high quality CVBs generation with the characteristics of high peak power, ultrashort pulse duration, and high mode purity.

Acknowledgement

This work was supported by the National Natural Science Foundation of China (NSFC) (Nos. 61905148, 61805278, and 61775146), Equipment Pre-research Field Foundation (No. 61404140304), China Postdoctoral Science Foundation (No. 2018M633704), and State Key Laboratory of Advanced Optical Communication Systems and Networks.

References

1. Q. Zhan, "Cylindrical vector beams: from mathematical concepts to applications," Adv. Opt. Photonics **1**, 1 (2009).
2. K. S. Youngworth and T. G. Brown, "Focusing of high numerical aperture cylindrical vector beams," Opt. Express **7**, 77 (2000).
3. Y. Kozawa, S. Sato, T. Sato, Y. Inoue, Y. Ohtera, and S. Kawakami, "Cylindrical vector laser beam generated by the use of a photonic crystal mirror," Appl. Phys. Express **1**, 022008 (2008).

4. X. Wang, J. Chen, Y. Li, J. Ding, C. Guo, and H. Wang, "Optical orbital angular momentum from the curl of polarization," Phys. Rev. Lett. **105**, 253602 (2010).
5. M. Beresna, M. Gecevičius, P. G. Kazansky, and T. Gertus, "Radially polarized optical vortex converter created by femtosecond laser nanostructuring of glass," Appl. Phys. Lett. **98**, 201101 (2011).
6. G. Milione, M. P. J. Lavery, H. Huang, Y. Ren, G. Xie, T. A. Nguyen, E. Karimi, L. Marrucci, D. A. Nolan, R. R. Alfano, and A. E. Willner, "4 × 20 Gbit/s mode division multiplexing over free space using vector modes and a *q*-plate mode (de)multiplexer," Opt. Lett. **40**, 1980 (2015).
7. S. C. McEldowney, D. M. Shemo, R. A. Chipman, and P. K. Smith, "Creating vortex retarders using photo-aligned liquid crystal polymers," Opt. Lett. **33**, 134 (2008).
8. T. Lei, M. Zhang, Y. R. Li, P. Jia, G. N. Liu, X. G. Xu, Z. H. Li, C. J. Min, J. Lin, C. Y. Yu, H. B. Niu, and X. C. Yuan, "Massive individual orbital angular momentum channels for multiplexing enabled by Dammann gratings," Light Sci. Appl. **4**, e257 (2015).
9. B. Ndagano, I. Nape, M. A. Cox, C. Rosales-Guzman, and A. Forbes, "Creation and detection of vector vortex modes for classical and quantum communication," J. Lightwave Technol. **36**, 292 (2018).
10. M. Dienerowitz, M. Mazilu, P. J. Reece, T. F. Krauss, and K. Dholakia, "Optical vortex trap for resonant confinement of metal nanoparticles," Opt. Express **16**, 4991 (2008).
11. S. C. Chu, T. Ohtomo, K. Tokunaga, and K. Otsuka, "Generating vortex laser beams by converting Ince–Gaussian laser beams with an astigmatic mode converter," in *Conference on Lasers and Electro-Optics/Pacific Rim* (Optical Society of America, 2009), p. TUP4_11.
12. D. Lin, N. Baktash, S. Alam, and D. J. Richardson, "106 W, picosecond Yb-doped fiber MOPA system with a radially polarized output beam," Opt. Lett. **43**, 4957 (2018).
13. M. Q. Mehmood, S. Mei, S. Hussain, K. Huang, S. Y. Siew, L. Zhang, T. Zhang, X. Ling, H. Liu, J. Teng, A. Danner, S. Zhang, and C.-W. Qiu, "Visible-frequency metasurface for structuring and spatially multiplexing optical vortices," Adv. Mater. **28**, 2533 (2016).
14. K. Saitoh, Y. Hasegawa, K. Hirakawa, N. Tanaka, and M. Uchida, "Measuring the orbital angular momentum of electron vortex beams using a forked grating," Phys. Rev. Lett. **111**, 074801 (2013).
15. X. Yi, X. Ling, Z. Zhang, Y. Li, X. Zhou, Y. Liu, S. Chen, H. Luo, and S. Wen, "Generation of cylindrical vector vortex beams by two cascaded metasurfaces," Opt. Express **22**, 17207 (2014).
16. S. Liu, S. Qi, Y. Zhang, P. Li, D. Wu, L. Han, and J. Zhao, "Highly efficient generation of arbitrary vector beams with tunable polarization, phase, and amplitude," Photon. Res. **6**, 228 (2018).
17. Z. Xie, T. Lei, F. Li, H. Qiu, Z. Zhang, H. Wang, C. Min, L. Du, Z. Li, and X. Yuan, "Ultra-broadband on-chip twisted light emitter for optical communications," Light Sci. Appl. **7**, 18001 (2018).
18. A. Matijošius, P. Stanislovaitis, T. Gertus, and V. Smilgevičius, "Formation of optical vortices with topological charge $|l| = 1$ and $|l| = 1/2$ by use of the s-waveplate," Opt. Commun. **324**, 1 (2014).
19. D. Lin, N. Baktash, M. Berendt, M. Beresna, P. G. Kazansky, W. A. Clarkson, S. U. Alam, and D. J. Richardson, "Radially and azimuthally polarized nanosecond Yb-doped fiber MOPA system incorporating temporal shaping," Opt. Lett. **42**, 1740 (2017).
20. Z. Bomzon, V. Kleiner, and E. Hasman, "Formation of radially and azimuthally polarized light using space-variant subwavelength metal stripe gratings," Appl. Phys. Lett. **79**, 1587 (2001).
21. D. Lin, J. Carpenter, Y. Feng, Y. Jung, S. Alam, and D. J. Richardson, "High-power, electronically controlled source of user-defined vortex and vector light beams based on a few-mode fiber amplifier," Photon. Res. **9**, 856 (2021).
22. X. Cai, J. Wang, M. Strain, B. J. Morris, J. Zhu, M. Sorel, J. L. O'Brien, M. G. Thompson, and S. Yu, Science **338**, 363 (2012).
23. Y. Liu, Y. Ke, J. Zhou, Y. Liu, H. Luo, S. Wen, and D. Fan, "Generation of perfect vortex and vector beams based on Pancharatnam–Berry phase elements," Sci. Rep. **7**, 44096 (2017).
24. A. V. Nesterov, V. G. Niziev, and V. P. Yakunin, "Generation of high-power radially polarized beam," J. Phys. D **32**, 2871 (1999).
25. D. Mao, Y. Zheng, C. Zeng, H. Lu, C. Wang, H. Zhang, W. Zhang, T. Mei, and J. Zhao," Generation of polarization and phase singular beams in fibers and fiber lasers," Adv. Photonics **3**, 014002 (2021).
26. F. Wang, F. Shi, T. Wang, F. Pang, T. Wang, and X. Zeng, "Method of generating femtosecond cylindrical vector beams using broadband mode converter," IEEE Photonics Technol. Lett. **29**, 747 (2017).
27. T. Wang, F. Wang, F. Shi, F. Pang, S. Huang, T. Wang, and X. Zeng, "Generation of femtosecond optical vortex beams in all-fiber mode-locked fiber laser using mode selective coupler," J. Lightwave Technol. **35**, 2161 (2017).
28. W. Zhang, K. Wei, D. Mao, H. Wang, F. Gao, L. Huang, T. Mei, and J. Zhao, "Generation of femtosecond optical vortex pulse in fiber based on an acoustically induced fiber grating," Opt. Lett. **42**, 454 (2017).